Loss of major nutrient sensing and signaling pathways suppresses starvation lethality in electron transport chain mutants

Alisha G. Lewis[a], Robert Caldwell[b], Jason V. Rogers[b], Maria Ingaramo[b], Rebecca Y. Wang[b], Ilya Soifer[b], David G. Hendrickson[b], R. Scott McIsaac[b], David Botstein[b], and Patrick A. Gibney[a,b,*]
[a]Department of Food Science, Cornell University, Ithaca, NY 14853; [b]Calico Life Sciences LLC, South San Francisco, CA 94080

ABSTRACT **The electron transport chain (ETC) is a well-studied and highly conserved metabolic pathway that produces ATP through generation of a proton gradient across the inner mitochondrial membrane coupled to oxidative phosphorylation. ETC mutations are associated with a wide array of human disease conditions and to aging-related phenotypes in a number of different organisms. In this study, we sought to better understand the role of the ETC in aging using a yeast model. A panel of ETC mutant strains that fail to survive starvation was used to isolate suppressor mutants that survive. These suppressors tend to fall into major nutrient sensing and signaling pathways, suggesting that the ETC is involved in proper starvation signaling to these pathways in yeast. These suppressors also partially restore ETC-associated gene expression and pH homeostasis defects, though it remains unclear whether these phenotypes directly cause the suppression or are simply effects. This work further highlights the complex cellular network connections between metabolic pathways and signaling events in the cell and their potential roles in aging and age-related diseases.**

Monitoring Editor
James Olzmann
University of California, Berkeley

Received: Jun 21, 2021
Revised: Oct 1, 2021
Accepted: Oct 5, 2021

INTRODUCTION

The mitochondrial electron transport chain (ETC) is a highly conserved biochemical pathway, well known for its role in respiratory ATP production. In this pathway, electrons supplied from NADH and $FADH_2$ are used to create a proton gradient across the inner mitochondrial membrane; this gradient drives proton flow through ATP synthase (ETC complex V), producing ATP from ADP. Beyond production of ATP, some components of the ETC appear to play other roles in regulating cellular physiology. For example, under conditions of mitochondrial stress, cytochrome *c* is released from the inner mitochondrial membrane where it can then act as a signaling protein to initiate apoptosis (Cai *et al.*, 1998; Ott *et al.*, 2001). While decades of intensive study have produced a significant body of knowledge surrounding the ETC, more-recent work suggests that there are still areas that remain unexplored (Nunnari and Suomalainen, 2012; Vafai and Mootha, 2012).

ETC function has been implicated in a wide array of human diseases. More than 150 diseases are associated with mitochondrial function, and most influence ETC function. These mitochondrial syndromes can affect any organ system, manifest at any age, and result in pathophysiology including stroke, deafness, renal failure, liver failure, and neuropathy, among others (Calvo and Mootha, 2010). Different mutations in individual complexes can manifest as different diseases, such as complex I mutations causing optic nerve atrophy or necrotizing encephalopathy (Nunnari and Suomalainen, 2012). In addition to these diseases, mitochondrial dysfunction is also considered one of the hallmarks of aging (López-Otín *et al.*, 2013). The diversity of disease phenotypes associated with mitochondrial mutations suggests a complex interaction with cellular regulatory networks, perhaps beyond those directly involved in producing ATP.

The yeast *Saccharomyces cerevisiae*, often described as a model eukaryote, has been used extensively for understanding mitochondrial biology, the ETC, and aging due to the high degree

This article was published online ahead of print in MBoC in Press (http://www.molbiolcell.org/cgi/doi/10.1091/mbc.E21-06-0314) on October 20, 2021.

Author contributions: P.A.G. and D.B. designed research; P.A.G., R.C., A.G.L., J.V.R., M.I., R.Y.W., I.S., and D.G.H. performed research and analyzed data; P.A.G., R.C., A.G.L., J.V.R., M.I., R.Y.W., I.S., D.G.H., R.S.M., and D.B. wrote the paper.

*Address correspondence to: Patrick A. Gibney (pag235@cornell.edu).

Abbreviations used: CFU, colony forming unit; ETC, electron transport chain; mtDNA, mitochondrial DNA; RNAPII, RNA polymerase II.

of conservation among many fundamental biological processes (Gibney *et al.*, 2013; Malina *et al.*, 2018). Aging in yeast is typically studied in two different ways: replicative aging and chronological aging (Longo *et al.*, 2013). Replicative aging refers to the capacity of a mother cell to produce daughter cells (in other words, the number of replications that occur before senescence). Chronological aging refers to the ability of a cell to survive after it has stopped growing. Survival is measured using the ability to form a colony or with a number of viability stains. The concept of chronological aging is intimately linked to nutrient starvation, although the growth-limiting nutrient may not always be explicitly defined or known.

Multiple studies have elucidated connections between the ETC and starvation-based phenotypes in yeast (Brauer *et al.*, 2005; Gresham *et al.*, 2011; Kwon *et al.*, 2015). Here we sought to comprehensively characterize the role of the ETC in starvation survival. We observed that a panel of different ETC mutants fail to survive starvation when the mutants are grown to saturation in standard minimal growth medium. This starvation lethality is associated with an overacidified cytosol and dysregulated gene expression compared with wild type cells. In an unbiased genetic suppressor screen, we found that loss of function mutations in major cellular nutrient sensing/signaling pathways (Ras/PKA, TORC1, PP2A) along with a number of gene expression regulators can prevent starvation lethality in these mutants. Together our results suggest that the ETC plays a critical regulatory role in mounting an appropriate response to starvation through communication with major nutrient sensing and signaling pathways in the cell.

RESULTS

Constructing and starving a set of ETC mutants

To assess the role of the ETC in starvation, we prepared a panel of yeast strains with disruptions in genes specifying each step of the pathway: the initial NADH dehydrogenase, complex II (succinate dehydrogenase), coenzyme Q, complex III (cytochrome bc_1), cytochrome *c*, complex IV (cytochrome *c* oxidase), and complex V (ATP synthase) (Figure 1A). Multiple genes encode mitochondrial NADH dehydrogenase enzymes in *S. cerevisiae*, including *NDE1* and *NDE2* (paralogues) and *NDI1*. Nde1/2 supply electrons to the ETC from NADH in the mitochondrial intermembrane space, while Ndi1 supplies electrons from mitochondrial matrix NADH. Notably in mammalian cells, NADH oxidation is performed by a large protein complex that also pumps protons into the intermembrane space, unlike Nde1/2 or Ndi1. By including disruptions at each biochemical step, this panel of strains allows for differentiation between step-specific and general loss of ETC function. To disrupt some steps, more than one gene was deleted from the genome, especially in the case of whole genome duplication paralogues (Figure 1A and Supplemental Figure 1). All of the final deletion strains were able to grow on glucose-containing plates but as expected could not grow on carbon sources that require respiration (glycerol and ethanol) (Figure 1B). Notably, galactose is a preferentially respired carbon source, and the ETC disruption mutants generally exhibited poor growth on galactose. One exception was the disruption of complex II by deleting *SDH1* and its paralogue *YJL045W*. This strain was able to grow much better than other ETC disruption mutants on galactose (Figure 1B). This is likely due to the specific role of complex II—it provides electrons in the form of $FADH_2$, and even without complex II, electrons can still enter the ETC via the mitochondrial NADH dehydrogenase enzymes (Nde1/2, Ndi1) from NADH. In liquid culture, the ETC mutants generally exhibit slower growth rates than wild type in YNB (yeast nitrogen base) + glucose, typically 40% slower (Figure 1C). However, ETC mutants have growth rates more similar to those of wild type cells in rich YPD medium (1% yeast extract, 2% bacto peptone, 2% dextrose), generally only about 15% slower (Figure 1D). It is not clear why this would be the case. An exception to this trend was *atp1*Δ, which grew more obviously slower in both types of media (Figure 1, C and D). Disruption of the mitochondrial ATP synthase is known to have broader effects than other ETC mutations because complex V regulates mitochondrial membrane potential, which in turn affects many of the essential mitochondrial membrane transporter activities (Martin *et al.*, 1991; Rehling *et al.*, 2003; Smith and Thorsness, 2005).

While many different conditions are used to measure starvation-based phenotypes, we opted to grow these strains in batch culture with a standard minimal medium (YNB + glucose; see *Materials and Methods* for details). Periodic time points were taken to measure survival based on colony forming units (CFUs). All ETC mutants exhibited significant starvation survival defects compared with wild type cells. Notably, the survival kinetics varied somewhat, with the complex II mutant strain (*sdh1*Δ *yjl045w*Δ) sustaining viability much longer than other mutants (Figure 2A). One possible explanation for this observation is that the complex II mutant strain still maintained some respiratory ability, as described above. One correlation often associated with loss of viability following starvation is an incomplete starvation response. This occurs when cells fail to sense or respond to the limiting nutrient, exemplified by auxotrophic cells starving for their auxotrophic requirement (Saldanha *et al.*, 2004; Boer *et al.*, 2008; Brauer *et al.*, 2008). One hallmark of such a defective starvation response is failure to properly arrest the cell cycle at G1/G0 (Saldanha *et al.*, 2004). In contrast, all the ETC mutants studied here had near-wild type levels of unbudded cells arrested at G1/G0 (Figure 2B).

ETC mutants exhibit deviations from typical post–diauxic shift gene expression

To better understand the mechanism underlying ETC mutant starvation survival defects, we examined gene expression throughout a growth curve in YNB + glucose. For this experiment we compared wild type with a subset of ETC mutants (*nde1*Δ *nde2*Δ *ndi1*Δ and *cox4*Δ). In addition to gene expression, we also measured standard growth parameters including cell count, cell size, and CFUs (Figure 3, A–C). ETC mutants exhibited wild type growth until the time when the wild type underwent the diauxic shift, which comprises an extensive remodeling of the patterns of gene expression that are necessitated by the absence of a fermentable carbon source once the glucose has been exhausted (Brauer *et al.*, 2005; Zampar *et al.*, 2013). When the wild type began the diauxic shift, the mutant cells exhibited significant decreases in cell size; after roughly 24 h the ETC mutants started losing the capacity to form new colonies (Figure 3, B and C). Gene expression changes were also evident starting at the point of diauxic shift—multiple clusters of genes had a divergent pattern compared with wild type (Figure 3D).

G0 term analysis of differentially regulated genes suggests that the ETC mutant strains are failing to perform appropriate signaling and response associated with diauxic shift gene expression (Supplemental Table 1). Many of the misregulated genes are annotated as being involved in cellular signaling and remodeling: biological regulation, protein modification, proteolysis, ubiquitin-dependent protein catabolism, and signal transducer activity. Because these observed deviations in gene expression are coincident with the diauxic shift, we compared the expression of the genes induced by diauxic shift in Brauer *et al.* (2005) to our RNA-seq results. We compared the 495 genes present in our data among the 520 genes identified by Brauer *et al.* as induced during diauxic shift and found that multiple

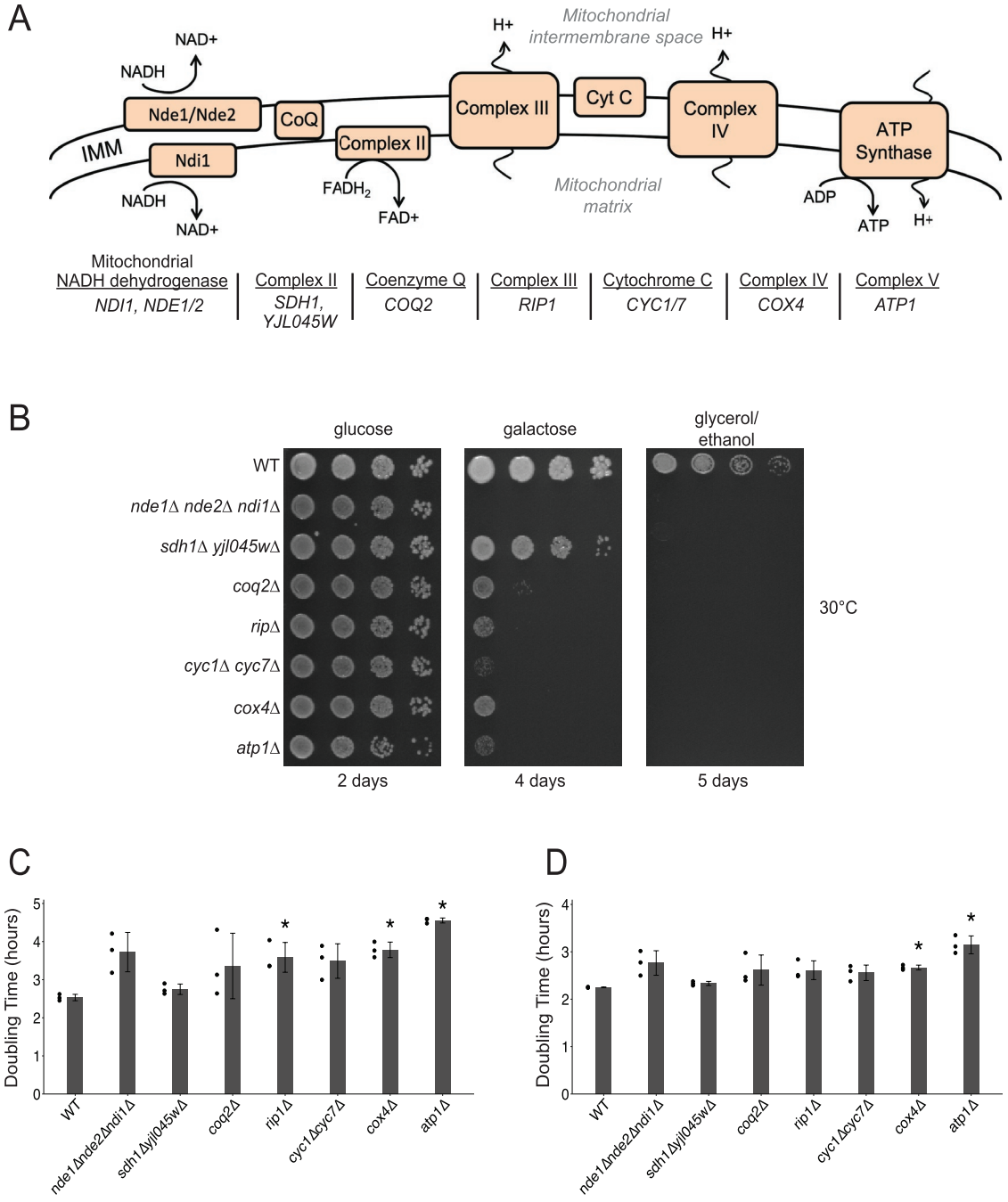

FIGURE 1: Construction and confirmation of ETC mutant strains. (A) Schematic of the yeast ETC and associated target genes for deletion. (B) Serial dilutions (1:10) of ETC deletion mutants were plated onto minimal media (YNB) with specified carbon sources for the indicated amount of time at 30°C before photographing. (C, D) Liquid culture growth rates of ETC mutants in YNB + glucose (C) and YPD (D) at 30°C performed in biological triplicate, as described in *Materials and Methods* (raw data points are shown to the left of each bar). The indicated doubling times are significantly different from those of wild type (*: uncorrected *p* value < 0.05).

clusters fail to induce in ETC mutants (Figure 3E). G0 term analysis of enriched genes in these clusters is unsurprisingly related to mitochondrial functions (Supplemental Table 2). Further, we used the REDUCE suite to estimate transcription factor activity from our gene expression data (Bussemaker *et al.*, 2001). Consistent with G0 term analysis of gene expression clusters, we predicted that the Cat8 transcription factor was less active in ETC mutants post–diauxic shift (Supplemental Figure 2). This prediction is consistent with the known role of Cat8 as a transcription factor involved in activating a wide range of respiratory metabolism genes post–diauxic shift (Haurie *et al.*, 2001). Further, Aft1 activity is also lower in ETC mutants post–diauxic shift; Aft1 is a transcription factor involved in iron utilization and homeostasis (Supplemental Figure 2) (Yamaguchi-Iwai *et al.*, 1995; Shakoury-Elizeh *et al.*, 2004). In methionine mutants that fail to survive methionine starvation, Aft1 transcription factor activity increases (Petti *et al.*, 2012). This is the opposite behavior observed

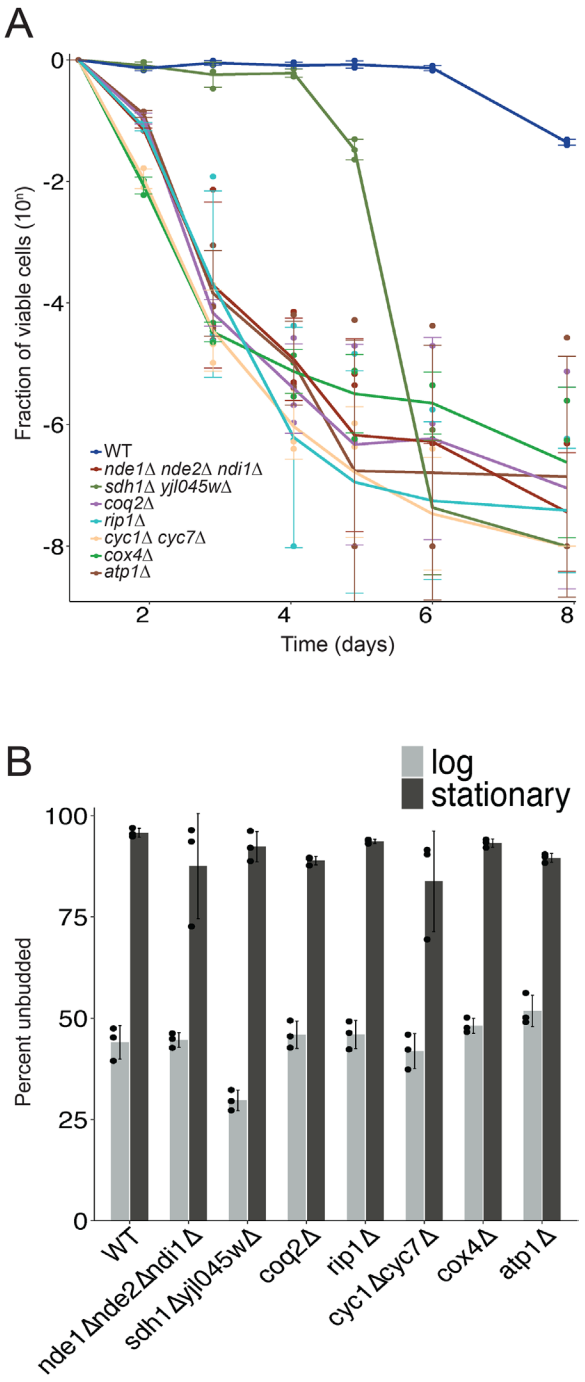

FIGURE 2: ETC mutants fail to survive batch growth in YNB + glucose. (A) Overnight cultures were pregrown in YNB + glucose and then subcultured into fresh YNB + glucose. Samples were taken at the indicated time points, and dilutions were plated to measure CFUs. (B) The fraction of unbudded cells was measured at both log phase and stationary phase (after 3 d in YNB + glucose). Shown is the average and standard deviation for three biological replicates, along with raw data plotted as points. A minimum of 300 cells were counted for each replicate.

in ETC mutant starvation, suggesting that Aft1 activity is not simply an indicator of lethal starvation conditions. These results highlight that removal of an ETC structural gene has wide-ranging impacts on gene expression, which implies that the ETC components play an active role in nutrient sensing/signaling.

Examination of potential nutrient deficit(s) in the YNB + glucose starvation regime

Growth to saturation in YNB + glucose is often used to induce starvation, though it is not clear which nutrient actually becomes limiting. To try to determine which nutrient is limiting and whether this is related to the starvation defect observed in ETC mutants, we first attempted to supplement excess nutrients into YNB + glucose and observe the effect on starvation of wild type cells compared with the mitochondrial NADH dehydrogenase mutant (*nde1Δ nde2Δ ndi1Δ*). Notably, only glucose had any effect, decreasing starvation-associated lethality (Supplemental Figure 3A). We next tested multiple concentrations of glucose in YNB + glucose, measuring survival over time. Interestingly, increasing glucose concentrations delayed, but did not prevent, cell death (Supplemental Figure 3B). Two exceptions to this included extremely high concentrations of glucose, 16% and 20%, though both conditions still retained residual glucose by the end of the experiment (Supplemental Figure 3, B and C). We also considered the possibility that continued exposure to ethanol after growth could affect survival of ETC mutants. Notably, replacement of conditioned media with YNB (no glucose) or YNB + ethanol (3% or 6%) equally delayed cell death, but the mitochondrial NADH dehydrogenase mutant (*nde1Δ nde2Δ ndi1Δ)* still died much faster than wild type (Supplemental Figure 3D). Finally, to test whether glucose is in fact limiting in YNB + glucose, we titrated various amounts of glucose or YNB mixture in minimal medium and measured the total cell density after 4 d of growth. It appears that adding excess YNB supports more cell growth than adding excess glucose, suggesting that standard YNB + glucose growth medium is not necessarily a simple carbon-limiting regime (Supplemental Figure 3E). The possibility that toxic molecules have accumulated has not been explicitly ruled out. Taken together, our results suggest that neither glucose alone, nor ethanol, is the sole cause of ETC mutant starvation survival defects. This is consistent with the gene expression results that suggest that lethality derives from a broader signaling defect associated with the diauxic shift, rather than a depleted nutrient per se.

ETC starvation defect is suppressed by mutations in major nutrient sensing and signaling pathways

To assess the role of the ETC in starvation survival, we performed an unbiased genetic suppressor screen to identify mutations that would allow an ETC mutant to better survive starvation. For each of the six strains that exhibited extremely poor survival in YNB + glucose, 96 independent cultures were inoculated and grown for 7 d. The entire culture volume was plated onto YPD to identify suppressors for 72 of the cultures, while the remaining cultures were used to estimate the mutation rate using the Luria–Delbruck fluctuation assay as recently adapted (Lang, 2018) (Supplemental Table 3). Potential suppressors were isolated and retested to confirm suppression activity. After this confirmation step, the remaining suppressor strains were used for whole genome sequencing to identify potentially causative suppressor mutations as described in *Materials and Methods*. A number of potentially causative suppressor mutations were identified, with many of them occurring in only a few biological pathways, including the Ras/PKA, TORC1, and PP2A pathways (Supplemental Table 4). Similar genes were mutated regardless of the ETC gene deletion, suggesting that these suppressor mutations repair the ETC starvation survival defect in general, and not through a particular ETC complex–specific mechanism. Similarly, Akdoğan *et al.* (2016) demonstrated that decreasing PKA activity can increase the lifespan of respiratory incompetent mitochondrial DNA (mtDNA) deficient cells, and

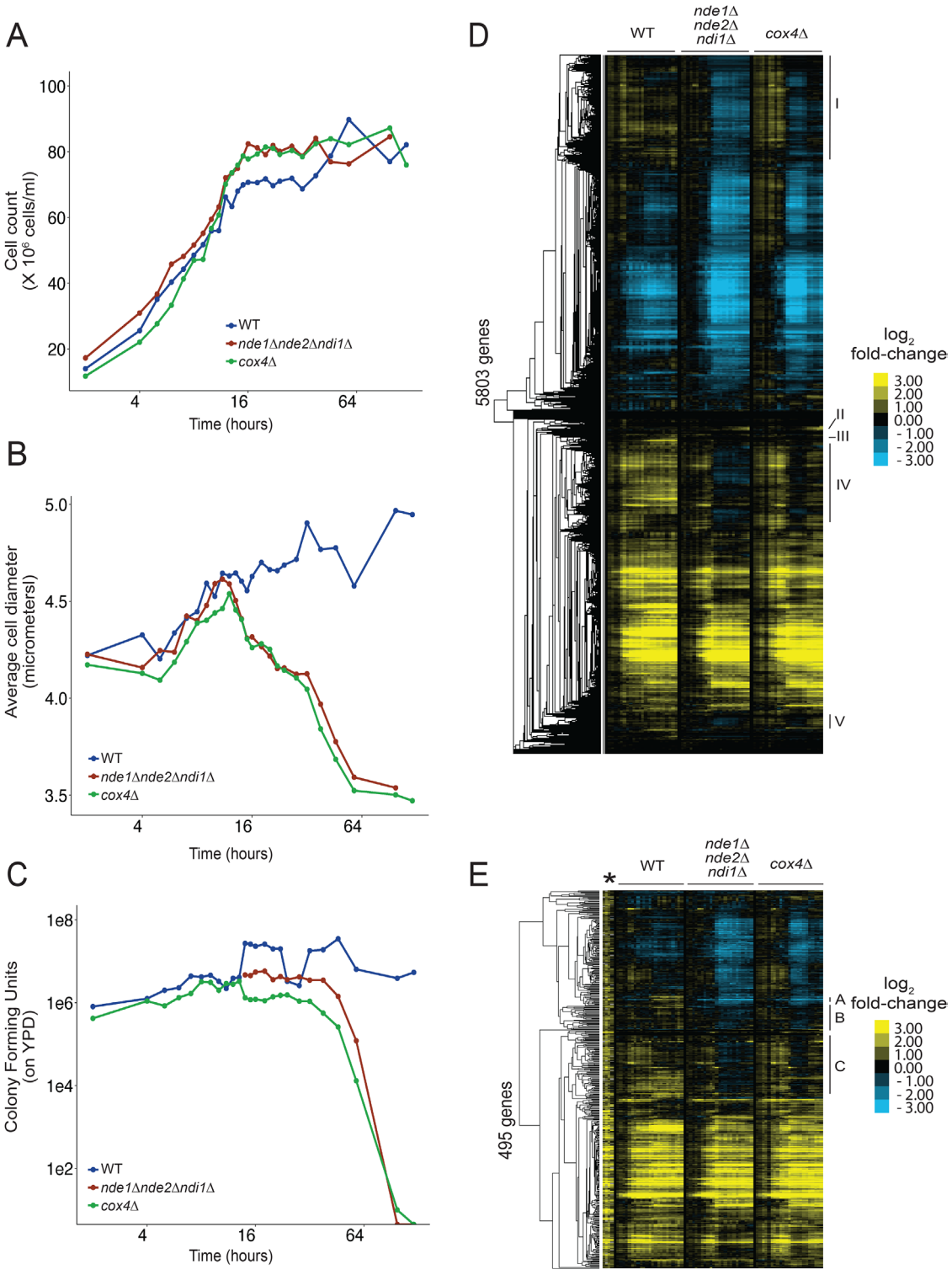

FIGURE 3: Gene expression defects in ETC mutants at diauxic shift. The indicated strains were grown in YNB + glucose at 30°C, and periodic samples were taken at 0, 2, 4, 5, 6, 7, 8, 9, 10, 11, 12, 13, 14, 15, 16, 18, 20, 22, 24, 28, 32, 38, 46, and 58 h to measure cell count (A), cell diameter (B), CFUs (C), and mRNA levels (D). (E) Comparison of genes induced at diauxic shift from *Brauer *et al.* (2005) with gene expression in ETC mutants. To the right of both heat maps, selected clusters for G0 term analysis (results in Supplemental Table 2) are labeled with either Roman numerals I–V (C) or letters A–C (D). Further details are provided in *Materials and Methods*.

Dolz-Edo *et al.* (2019) demonstrated that PKA activity regulates survival of stationary-phase cells grown in buffered, supplemented minimal media. Further, our results are in agreement with observations that decreased TORC1 pathway signaling has been shown to increase the chronological lifespan in *S. cerevisiae* (Powers *et al.*, 2006).

Gene	Source	Function	Mutation[a]	Del.[b]
IRA1	This work	Ras/PKA; GTPase-activating protein for Ras	A1657V	No
IRA2	This work	Ras/PKA; GTPase-activating protein for Ras	Multiple[c]	No
CDC25[d]	This work	Ras/PKA; GEF for Ras	Multiple[c]	n.d.[e]
RAS1	This work	Ras/PKA; GTP-binding protein	D126N, A25P	No
RAS2	This work	Ras/PKA; GTP-binding protein	Null	Yes
CYR1[d]	This work	Ras/PKA; adenylate cyclase	Multiple[c]	n.d.[e]
SRV2	This work	Ras/PKA; cyclase-associated protein	M8I	Yes
TPD3[d]	This work	PP2A; regulatory subunit A of PP2A	Multiple[c]	n.d.[e]
CDC55	This work	PP2A; regulatory subunit B of PP2A	Null	Yes
RTS1	This work	PP2A; regulatory subunit B of PP2A	Null	Yes
PPM1	Boer *et al.*, 2008	PP2A; methylates/regulates PP2A	n/a[f]	Yes
PPH21	This work	PP2A; catalytic subunit; *PPH22* paralogue	n/a[f]	Yes
PPH22	This work	PP2A; catalytic subunit; *PPH21* paralogue	n/a[f]	Yes
TOR1	Boer *et al.*, 2008	TOR; subunit of TORC1	n/a[f]	Yes
TCO89	This work	TOR; subunit of TORC1	Null	Yes
MDS3	This work	TOR; putative TOR regulator	Null	Yes
TUS1	This work	TOR; Rho1 GEF, suppressor of *tor2*	Y954H	Yes
SCH9	Boer *et al.*, 2008	TOR; kinase involved in nutrient signaling	n/a[f]	Yes
CCR4	This work	CCR4-NOT; gene expression regulator	Null	Yes
CDC39[d]	This work	CCR4-NOT; gene expression regulator	S1903ns[g]	n.d.[e]
SRB8	This work	RNAPII mediator subunit; glucose repression	Null	Yes
SSN8	This work	Cyclin-like RNAPII component; glucose repression	Null	Yes
PHO85	This work	Cyclin-dependent kinase; nutrient response	ΔF158-A176	Yes

RNAPII, RNA polymerase II.
[a]Specific mutation or mutation category observed.
[b]Suppression confirmed by gene deletion.
[c]See Supplemental Table 4 for detailed list of mutations.
[d]Essential gene.
[e]Not determined (because gene is essential).
[f]These genes were added to this confirmation due to observation in previous study or association with identified pathway (rather than identification from this genetic screen).
[g]ns indicates a nonsense allele (insertion of a stop codon).

TABLE 1: ETC suppressor confirmation.

Many of the suppressor mutations, though not all, were predicted loss-of-function mutations (Supplemental Table 4). We confirmed suppression activity by constructing deletion mutants for each nonessential suppressor gene in combination with two different ETC genes (Table 1). We recapitulated suppression for the vast majority of these deletion mutations, with a few exceptions; for example, deletion of *IRA1* and *IRA2* did not cause suppression, though when we observed mutations in these genes they almost always occurred in combination with other mutations in the Ras/PKA pathway (Figure 4, A and B, and Supplemental Table 4). The strength of suppression varied between mutants, and individual suppressor deletions alone exhibited variation in growth rate (Supplemental Figure 4). In addition to mutations in major nutrient sensing/signaling pathways, we confirmed a number of other suppressors that are involved with gene expression regulation (*CCR4*, *SRB8*, *SSN8*) and a cyclin-dependent kinase involved with nutrient sensing/signaling (*PHO85*). While ETC mutants alone did not exhibit bud index defects during starvation, we also examined whether independent suppressor mutations alone exhibit any defects in cell cycle arrest in stationary phase in YNB + glucose. We did not find any trends in bud index related to suppression of starvation lethality (Supplemental Figure 5). Taking the data together, we have identified a diverse catalogue of mutations that can suppress this ETC mutant starvation survival defect, implicating the ETC as having a role in regulating the appropriate response to starvation.

Some ETC suppressor mutants are specific to starvation of ETC mutants, while others affect starvation in general

A previous genetic screen to identify suppressors of leucine starvation identified TORC1 and PP2A genes but not Ras/PKA genes (Boer *et al.*, 2008). While identical pathways were implicated by both screens, Boer *et al.* (2008) identified a number of pathway component genes that we did not observe as suppressors of ETC mutant starvation lethality, including *PPM1*, *TOR1*, and *SCH9*. We therefore directly tested and confirmed that these three gene deletions suppress ETC starvation lethality, demonstrating that our suppressor screen was not saturating (Table 1 and Figure 4). We also wanted to determine whether the different classes of ETC suppressor mutants were general starvation suppressors or specific to ETC starvation lethality. To perform this experiment, we selected a subset of

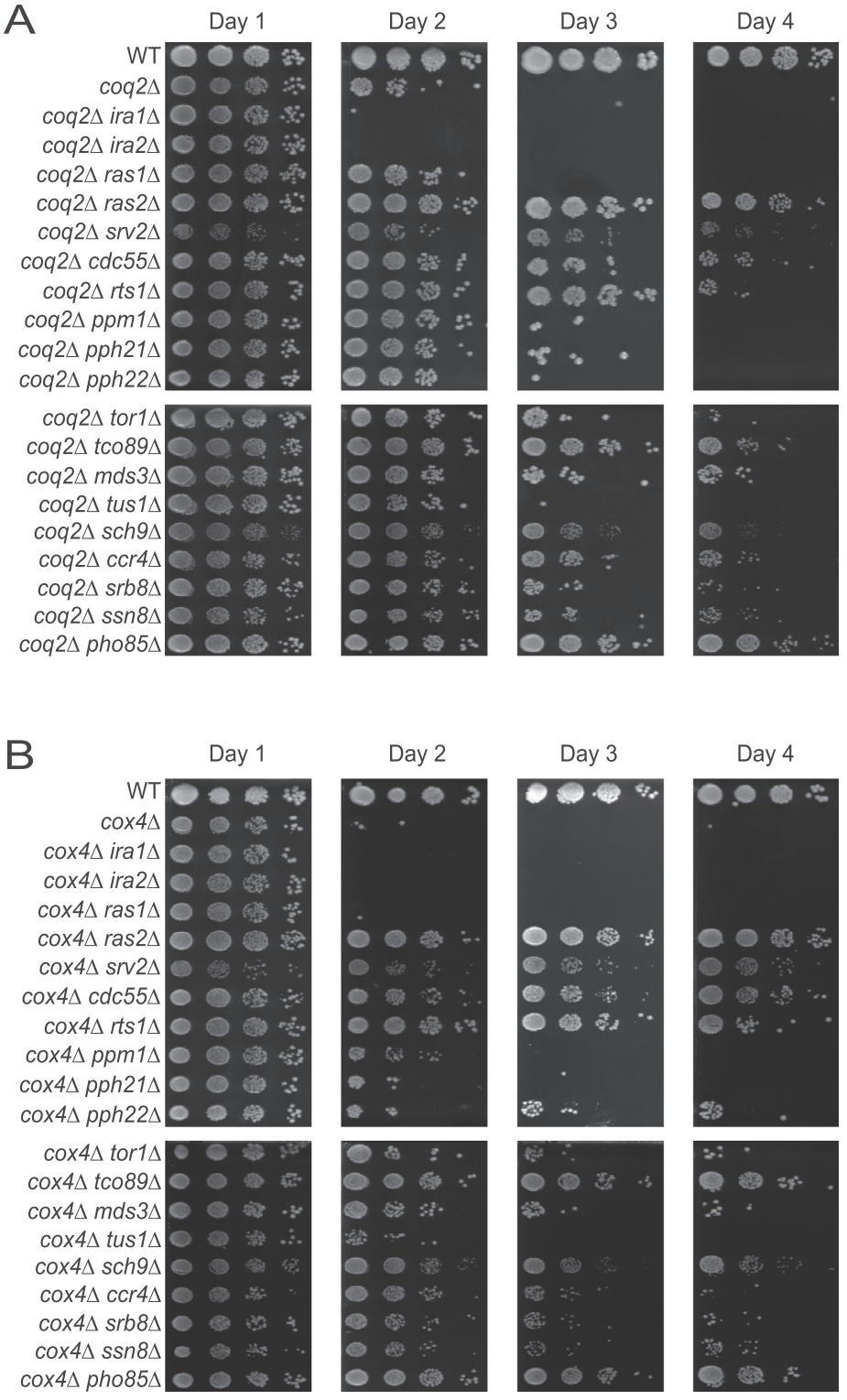

FIGURE 4: Confirmation of ETC starvation survival suppressors. The indicated strains were grown overnight in YNB + glucose and then subcultured in YNB + glucose. Aliquots were removed at the indicated time points, and 10-fold serial dilutions were spotted onto YPD to assess CFU. YPD plates were incubated at 30°C for 3 d before photographing. Double gene deletions are indicated with *coq2*Δ (A) and *cox4*Δ (B).

suppressor gene deletions representing each major pathway identified and then deleted *LEU2* to make them auxotrophic for leucine. As the goal was to examine whether the suppressor gene deletions could also suppress leucine starvation, these strains did not contain the ETC gene deletions and contained only a suppressor gene deletion along with *leu2Δ0*. We used these strains to perform leucine starvation essentially as described (Boer *et al.*, 2008). In the case of the Ras/PKA pathway, neither *ras2*Δ nor *srv2*Δ was able to suppress leucine starvation lethality (*srv2*Δ exacerbates lethality) (Figure 5A). For the TORC1 pathway, *tor1*Δ was able to suppress leucine starvation lethality, as seen in Boer *et al.* (2008) (Figure 5B). In contrast, *mds3*Δ was unable to suppress leucine starvation lethality (Figure 5B). For suppressors related to PP2A, *rts1*Δ only partially suppressed the lethality of leucine starvation, while *ppm1*Δ fully suppressed leucine starvation lethality, again as seen in Boer *et al.* (2008) (Figure 5C). Finally, among our remaining suppressors tested, *pho85*Δ suppressed leucine starvation lethality, while *ccr4*Δ, *srb8*Δ, and *ssn8*Δ failed to suppress the lethality of leucine starvation (Figure 5D). These results suggest that some of these pathway components are specific for ETC mutant starvation survival, rather than playing a general role in all cellular starvation conditions, and that the PKA pathway might have a unique or specific role during ETC-associated starvation.

ETC suppressor mutations display a constitutive stress response before diauxic shift

Because the ETC mutants exhibited altered gene expression patterns during the diauxic shift (Figure 3E), we asked whether the ETC suppressor mutants rescued viability by also restoring the normal diauxic shift gene expression pattern. To this end, we performed transcriptional profiling of cells before and at two time points after the diauxic shift in a wild type strain, two ETC mutants (*cox4*Δ and *coq2*Δ), and four ETC mutant suppressors (*ras2*Δ and *rts1*Δ in both the *cox4*Δ and *coq2*Δ backgrounds). To examine differential patterns of gene expression, we used the software Sleuth as described in *Materials and Methods*. One of the most straightforward suppression patterns would be genes that are induced during the diauxic shift in wild type but not in the ETC mutants and induced to wild type levels again in the ETC mutant suppressors. We identified 134 genes that changed significantly differently in both *cox4*Δ and *coq2*Δ compared with wild type after the diauxic shift. Contrary to expectations, only a small subset of these genes (17 of 134; 13%) showed any sign of restoration of wild type levels in the suppressor mutants (Figure 6A). These genes shared no significant G0 term enrichment. Of these 17 genes, only two fit the pattern of failing to induce in the *cox4*Δ and

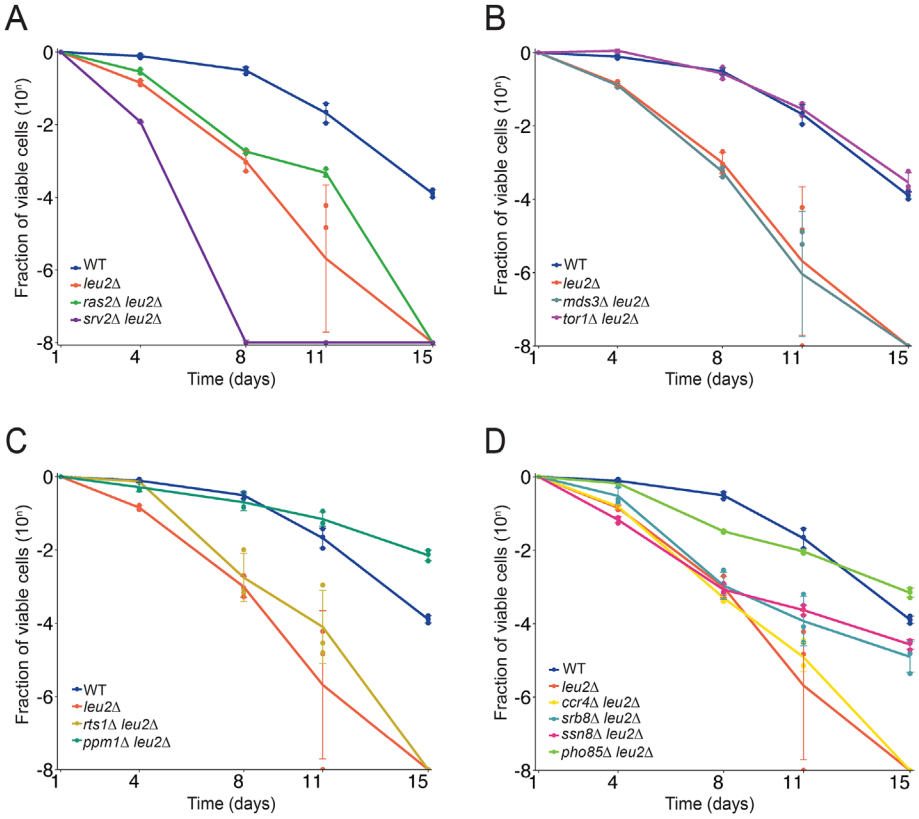

FIGURE 5: A subset of ETC mutant starvation survival defect suppressors also suppress leucine starvation, while others do not. To starve cells for leucine, the indicated strains containing *leu2Δ0* combined with suppressor gene deletions were grown overnight in leucine-limiting medium and then subcultured into the same medium. Aliquots were removed at the indicated time points, and 10-fold serial dilutions were plated onto YPD to assess CFU. Line plots represent the average values and standard deviation from three biological replicates, with raw data represented as points. Suppressors in the (A) Ras/PKA pathway, (B) Tor pathway, and (C) PP2A pathway. (D) Suppressors related to gene expression regulation and *PHO85*.

*coq2*Δ mutants and reverting toward wild type levels in the suppressor mutants: *MSN4* and *OM14*. Msn2 and Msn4 are paralogous transcription factors critical for activating the stress response during the diauxic shift, and Om14 is a mitochondrial outer membrane protein. Although this is a short list, these genes could be critical for maintaining viability during the transition to stationary phase. Extending this analysis to pre–diauxic shift, we identified 180 genes that changed expression in both *cox4*Δ and *coq2*Δ compared with wild type before the diauxic shift. Of these, 38 (21%) restored or partially restored a wild type expression pattern in the suppressors (Figure 6B). These genes were enriched for the G0 term "cellular carbohydrate biosynthetic process" (six of 38; *GLC3*, *GSY1*, *GSC2*, *INM1*, *GPP1*, and *GAS1*).

As another potential suppression mechanism, we considered a bypass pattern of gene expression in which transcript levels did *not* change differently in both *cox4*Δ and *coq2*Δ after the diauxic shift compared with wild type but did in the ETC suppressor mutants. In contrast to the small number of genes exhibiting a suppressive pattern, 790 genes fit the bypass pattern, and 706 of these were up- or down-regulated during log phase, before the diauxic shift occurred. Most of these genes appeared to be up- or down-regulated naturally during the diauxic shift in wild type and were enriched for ribosome biogenesis factors, aerobic respiration, and other terms generally linked to growth rate and stress response.

Based on these observations, it appears that the ETC suppressor mutants have a constitutive stress response that may provide protection against the altered cellular environment encountered during the diauxic shift remodeling of gene expression in the ETC mutants. Because of the observed restoration of *MSN4* expression and the apparent constitutive stress response activity, we asked whether Msn2/4 signaling, or another transcription factor activity, is altered in the ETC suppressor mutants. We used the REDUCE suite to infer transcriptional activity and searched for transcription factor activity patterns consistent with a suppressor or bypass mechanism (Supplemental Figure 6). Consistent with our other results, Msn2/4 activity appeared to be up-regulated prematurely during log phase in the suppressor mutants (Figure 6C), although the effect was more modest in the *rts1*Δ mutants. In summary, the ETC suppressor mutants exhibit a constitutively active stress response, likely mediated by Msn2/4 signaling, and this may confer the observed restoration of viability in the ETC mutants post–diauxic shift.

ETC mutations affect cytosolic pH during starvation

Recent work has suggested that cytosolic pH regulation is connected to many aspects of cell biology, including growth phase, meiosis, stress response, nutrient sensing/signaling, and aging (Ohkuni *et al.*, 1998; Dechant *et al.*, 2010; Orij *et al.*, 2011; Henderson *et al.*, 2014). To better understand the phenomenon of ETC mutant starvation survival, we also examined cytosolic pH during starvation of one ETC mutant (*cox4*Δ) and compared these results to those of wild type cells. To measure the cytosolic pH, we took advantage of a pH-sensitive fluorescent protein, pHluorin2 (Mahon, 2011). pHluorin2 has bimodal excitation peaks at 395 and 475 nm and an emission maximum for both at 509 nm; the ratio of emission at each excitation is pH sensitive and can therefore be used to estimate pH in cellular compartments (Mahon, 2011). As previously observed, we noted that wild type cells exhibit a decrease in cytosolic pH corresponding to cessation of growth (Figure 7) (Joyner *et al.*, 2016). We noted that the *cox4*Δ mutant also exhibited a decrease in cytosolic pH, though it was more severe than in wild type cells (Figure 7). To determine whether the genetic suppressors also suppressed the cytosolic pH phenotype, we tested a suppressor mutation from each category of major nutrient sensing/signaling pathways (Ras/PKA, TORC1, and PP2A). In each case, the cytosolic pH decrease had slower kinetics and also an intermediate value between those of wild type and *cox4*Δ (Figure 7). Notably, the lower detection limit of pHluorin2 appeared to be near a pH value of 5.5, which was also the value we detected for the *cox4*Δ mutant (Supplemental Figure 7).

To validate our results, we performed an essentially identical experiment with a different pH-sensitive fluorescent molecule that has a lower pH detection range, mScarlet (Bindels *et al.*, 2017). For mScarlet, the fluorescence lifetimes are related to pH (Bindels *et al.*, 2017). Our calibration curve with mScarlet demonstrated an effective

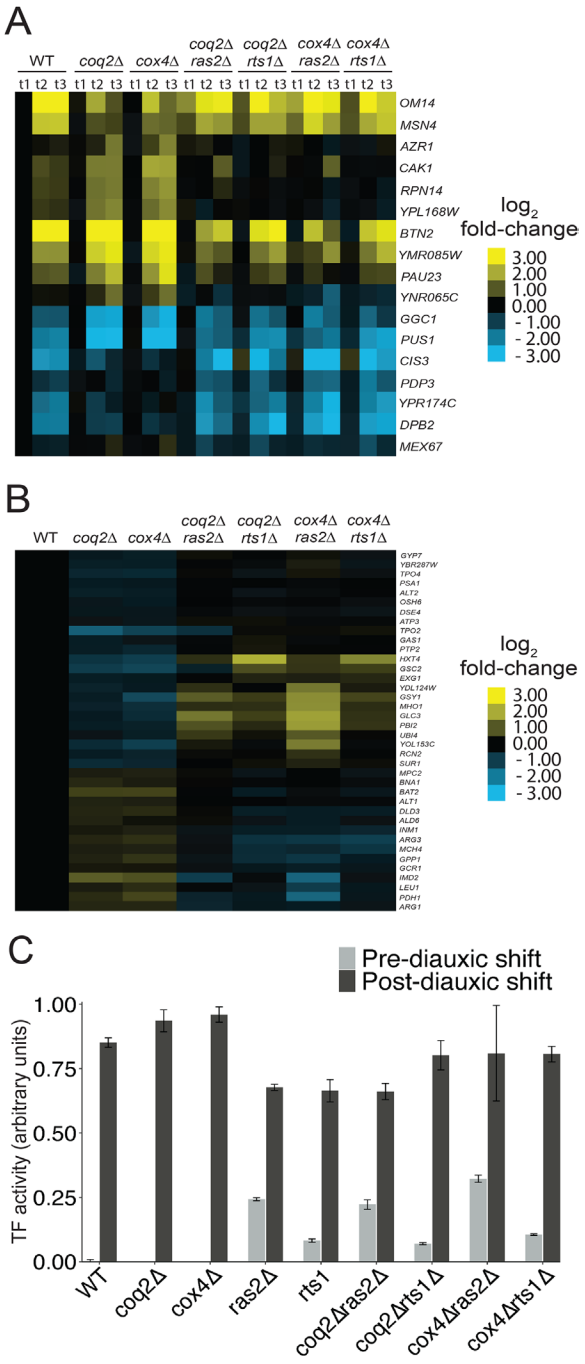

FIGURE 6: ETC mutant suppressors partially restore wild type gene expression and cause a constitutive stress response before diauxic shift. Results of differential gene expression for potential suppression determinants based on postdiauxic gene expression (A) or prediauxic gene expression (B). Samples from a YNB + glucose time course were collected for RNA extraction at one point before diauxic shift (t1, 4 h) and two points after diauxic shift (t2 and t3, 16 and 20 h, respectively). RNA extraction, sequencing, and differential gene expression analysis were performed using SLEUTH as described in *Materials and Methods*. (C) Msn2/4 activity was estimated for each of the indicated strains both pre–diauxic shift and for the average of both post–diauxic shift time points. Transcription factor activity was estimated using the REDUCE suite as described in *Materials and Methods*.

pH range from 4 to 6 (Supplemental Figure 8). As seen with pHluorin2, the *cox4*Δ mutant exhibited a much lower pH than that of wild type cells, which was restored by the three tested suppressor mutations (Supplemental Figure 9). Notably, the cytosolic pH detected using mScarlet for *cox4*Δ was lower than that observed with pHluorin2 after starvation (average pH = 4.4 with mScarlet compared with pH = 5.5 with pHluorin2). This suggests that some of the lower pHluorin2 values were inaccurate due to its associated linear range, which validated the decision to confirm these results with an independent system. Taken together, these results demonstrate that pH homeostasis is impaired in starving ETC mutants and that suppressors of ETC starvation defects also partially restore pH homeostasis. It remains unclear whether pH homeostasis is a cause or effect of misregulated signaling in these cells.

DISCUSSION

The goal of this analysis was to examine the role of the ETC in starvation lethality, which is often used as a model of chronological aging in yeast. We began by systematically deleting subunits within the different complexes of the ETC to yield a panel of respiratory incompetent ETC mutants. Next, we subjected the entire panel to starvation by growing the strains in YNB + glucose and measured survival along with a number of other cellular parameters. We observed that ETC mutants are unable to survive starvation in YNB + glucose compared with wild type, exhibit defective diauxic shift gene expression, and fail to regulate cytosolic pH. Further, we identified mutations in pathways such as Ras/PKA, TORC1, and PP2A, which suppress the ETC starvation lethality phenotype. Together these results suggest a role for the ETC in starvation response regulation and also shed light on major pathways that are likely involved during ETC-regulated starvation survival.

Genetic and environmental factors regulate ETC mutant survival

Our ETC mutant starvation lethality phenotype is supported by similar observations in multiple publications that have also observed starvation and/or aging phenotypes associated with ETC mutants. For example, a systematic study of yeast genes required for starvation survival identified mitochondrial genes as important for phosphate starvation but not leucine starvation (Gresham *et al.*, 2011). Another group demonstrated that only a fraction of 73 tested ETC gene deletions had decreased lifespan in both chronological and replicative models of aging, while multiple other mutants had no observable defects (Hacioglu *et al.*, 2012). McCormick *et al.* (2015) systematically examined the nonessential yeast gene deletion collection for mutants with an increased replicative lifespan and among long-lived mutants found four ETC mutants including succinate dehydrogenase (*SDH1*, *SDH2*), cytochrome *C* (*CYC1*), and mitochondrial ATP synthase (*ATP17*) gene deletions. Kwon *et al.* (2015) examined 33 ETC gene deletions for starvation survival, respiratory ability, mitochondrial membrane potential, ATP levels, and superoxide levels. Many of the 33 mutants exhibited starvation lethality, though some mutants exhibited wild type survival despite being respiratory incompetent. While these publications link ETC gene mutations with starvation survival and aging, Gresham *et al.* (2011) highlight that starvation environment is relevant as ETC mutants survive normally during leucine starvation but rapidly lose viability in phosphate starvation. This observation is bolstered by other studies that demonstrate the limiting nutrient during starvation strongly dictates survival kinetics (Culbertson and Henry, 1975; Boer *et al.*, 2008; Petti *et al.*, 2011, 2012)

Failed diauxic shift gene expression in ETC mutants

Transition from glucose fermentation to ethanol respiration and eventually stationary phase is associated with cellular changes such

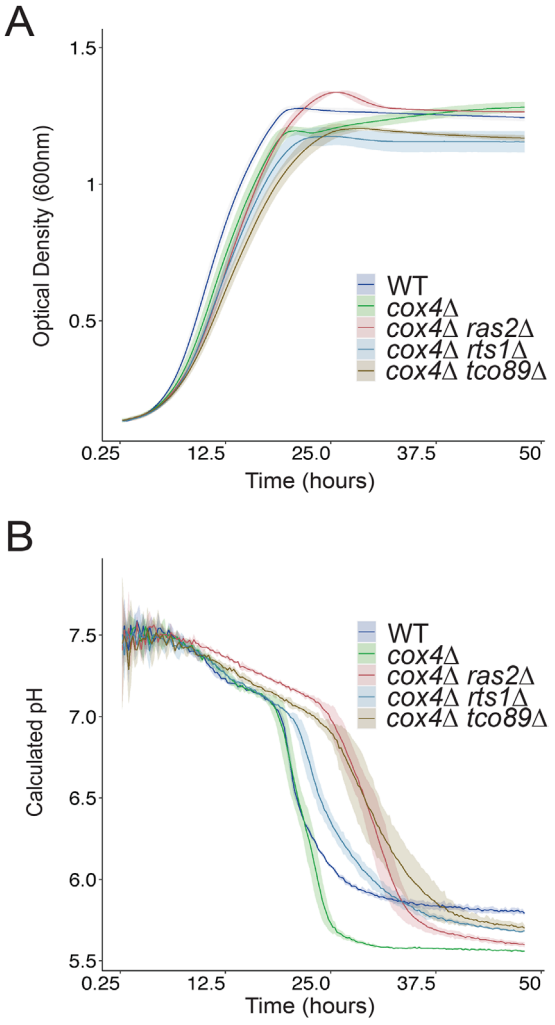

FIGURE 7: ETC mutant suppressors partially restore intracellular pH homeostasis. The indicated strains containing pHluorin2 were grown in YNB + glucose in a plate reader at 30°C with constant shaking as described in *Materials and Methods*. (A) Plate reader growth curve (OD_{600}). (B) Calculated pH curves based on pHluorin2 calibration (Supplemental Figure 7). The line indicates the average of three biological replicates, while the lower-intensity color represents the standard deviation.

as thickening of the cell wall and increasing mitochondrial content, as well as activating genes associated with respiratory metabolism and stress resistance (Werner-Washburne *et al.*, 1993). Apart from the mitochondrial network rapidly occupying a greater volume of the cell, proteins associated with mitochondrial function such as those of the tricarboxylic acid cycle, ETC, and mitochondrial transporters are up-regulated during diauxic shift (Di Bartolomeo *et al.*, 2020). Along with an up-regulation of mitochondrial-associated protein synthesis and physiological/morphological changes, the activity of key nutrient sensing/signaling pathways is also affected during the diauxic shift. For example, PKA, TORC1 and the Rim15 protein kinase regulate entry from the exponential phase to the diauxic and stationary phase (Galdieri *et al.*, 2010).

We observed a subset of genes failing to exhibit wild type responses to diauxic shift in both ETC mutants tested. Many genes that were up-regulated during diauxic shift in wild type cells are either not increased or decreased in ETC mutants. Based on transcription factor activity analysis, it appears that Cat8 and Aft1 transcription factors are the major drivers of this defect. It is not clear how the absence of a single metabolic pathway enzyme has such wide-ranging effects on gene expression, and this may not be a typical response. During leucine limitation, a leucine metabolism mutant (*leu2-3leu2-11*) was still able to induce the leucine genes (Brauer *et al.*, 2008) (Supplemental Figure 10). Similarly, deletion of methionine biosynthetic enzyme genes, *MET6* or *MET13*, did not impede expression of other genes in methionine/sulfur metabolism during methionine starvation (Petti *et al.*, 2011, 2012) (Supplemental Figure 10). Notably this is not the case for uracil limitation, though expression of *URA* genes may not be dependent on uracil levels as previously suggested (Saldanha *et al.*, 2004) (Supplemental Figure 10). In contrast, it seems that disruption of the ETC affects cellular physiology in more ways than by simply blocking oxidative phosphorylation. The expression of oxidative metabolism genes appears to be regulated by the presence of an active ETC, though the molecular mechanism of this remains unclear.

Examination of ETC suppressor gene expression led to the observation that ETC suppressors have up-regulated Msn2/4 activity compared with ETC mutants alone. Msn2/4 comprise a pair of partially functionally redundant transcription factors that aid in cellular stress response by controlling the expression of stress-responsive genes (Martinez-Pastor *et al.*, 1996; Estruch, 2000; Gasch *et al.*, 2000). The Msn2/4 transcription factor regulates diauxic shift–induced genes and is a known target of Ras/PKA regulation, indicating an important role in starvation survival (Boy-Marcotte *et al.*, 1998; Görner *et al.*, 2002). While there has been some debate about the role of TORC1 signaling in regulating Msn2/4, PP2A activity is both connected to TORC1 activity and a known regulator of Msn2/4 nuclear localization and chromatin binding (Santhanam *et al.*, 2004; Powers *et al.*, 2006; Broach, 2012; Reiter *et al.*, 2013). Notably the examined suppressor mutations did not increase the activity of Cat8 or Aft1. Together these results further suggest that many of our suppressors act downstream of the ETC nutrient sensing/signaling defect by activating the stress response through Msn2/4, though it is not clear why there is variability in ETC starvation survival compared with leucine starvation survival for individual suppressor mutants.

Cytosolic pH dysregulation is associated with ETC mutant survival defects

Cytosolic pH is highly regulated and important for the maintenance of various cellular activities. Cytosolic pH is associated with growth rate, diauxic shift, carbon source utilization, protein interactions, and mitochondrial functions and has been suggested to play a role in nutrient sensing/signaling (Orij *et al.*, 2009, 2011, 2012; Dechant *et al.*, 2010; Isom *et al.*, 2018; Leemputte *et al.*, 2020). For example, glucose-starved cells display a drop in cytosolic pH (Martínez-Muñoz and Kane, 2008; Orij *et al.*, 2009; Joyner *et al.*, 2016). Additionally, ethanol stress and associated oxidative and cell wall stress also result in decreased cytosolic pH (Charoenbhakdi *et al.*, 2016). It is likely that nutrient sensing and signaling pathways such as PKA and TORC1 act together in the regulation of pH homeostasis, as PKA activity has been associated with starvation-induced cytosolic pH changes and TORC1 is associated with the H^+-ATPase Pma1, a major regulator of cytosolic pH (Deprez *et al.*, 2018; Saliba *et al.*, 2018; Dolz-Edo *et al.*, 2019). Acidification of cytosolic pH results in a change of the cytoplasmic state from fluid to solid-like (Munder *et al.*, 2016). Cytoplasmic transition to this solid-like state appears to be important for cells to survive starvation stressors such as limited glucose availability (Munder *et al.*, 2016). We recapitulated the observation that diauxic shift is coincident with a cytosolic pH drop of roughly 1 pH unit in wild type cells. As ETC mutants display a

markedly reduced cytosolic pH and because ETC suppressors are able to restore a more normal cytosolic pH, it is possible that ETC mutant survival is related to inappropriate regulation of this cytoplasmic phase transition. The exacerbated decrease of cytosolic pH in the ETC mutants could be due to failed nutrient sensing/signaling through the PKA pathway. While the mechanism by which PKA controls cytosolic pH is not known, it is also possible that irregular PKA activity in ETC mutants together with decreased ATP production results in Pma1 inactivation, resulting in a lowered ability to pump protons out of the cell, affecting the cytosolic pH and TORC1 activity. ETC suppressors may bypass the failed nutrient sensing/signaling and act as if cells are stressed, supported by our observation that suppressors have increased Msn2/4 activity, allowing them to maintain H^+ concentrations similar to that of wild type. Further, ETC suppressors may exhibit slower pH changes due to similar alterations in stress response activity and/or altered Pma1 activity.

Conclusions

Together these results suggest that the ETC mutants fail to survive because of a cellular signaling failure of the onset of the extensive physiological changes associated with the diauxic shift (such as pH changes) in the absence of respiratory competence. The details of this signaling remain unclear. One possibility is that this happens via retrograde signaling, a mitochondrial stress response mechanism. Mitochondrial dysfunction triggers retrograde signaling to signal mitochondrial dysfunction to the nucleus, which in turn activates a number of pathways to mitigate such a perturbation such as a rewiring of nitrogen metabolism (Liu and Butow, 2006; Jazwinski, 2013; Da Cunha *et al.*, 2015). Retrograde signaling is also connected to the Ras/PKA and TORC1 pathways (Matsuura and Anraku, 1993; Kirchman *et al.*, 1999; Liu *et al.*, 2001; Kawai *et al.*, 2011). Together these results indicate that retrograde signaling is a possible intermediary between the ETC role in starvation survival and major nutrient pathways. Future work is required to delineate the network connecting the ETC to events upstream of stress response activation, including determining the ETC role in modulating Ras/PKA or other pathways, along with its role in activating appropriate diauxic shift response genes.

MATERIALS AND METHODS

Yeast media, growth, and starvation

Yeast cell growth and standard laboratory manipulations were performed as described. All media used were either minimal (0.67% YNB with ammonium sulfate without amino acids plus 2% indicated carbon sources) or rich (2% bacto peptone, 1% yeast extract, 2% indicated carbon sources). Exceptions are noted in the text (for example, YPGE medium contained 2% bacto peptone, 1% yeast extract, 3% glycerol, and 2% ethanol). YNB + glucose is used throughout the text to indicate minimal medium containing 2% glucose (this is also commonly referred to as synthetic dextrose, or SD). All media components described are indicated as weight per volume. Cell concentration was monitored by measuring the optical density at 600 nm (Thermo Fisher Scientific Genesys 6 UV-Vis Spectrophotometer). Cell concentration was also monitored, along with cell volume, using a Z2 Coulter Counter (Beckman Coulter). Bud index was measured by counting at least 300 cells using a hemocytometer. Strain growth comparisons using pronging were performed by growing overnight cultures in the indicated media and then collecting, washing, and diluting them to an OD_{600} of 1.0. From this solution, a series of 10-fold serial dilutions were prepared in a 96-well plate and then spotted onto the indicated growth media using a 48- or 96-pin replicating tool (Sigma-Aldrich). Standard YNB + glucose starvations were performed by diluting YNB + glucose overnight cultures into fresh YNB + glucose and then allowing them to grow to saturation. Leucine starvation was performed essentially as described in Boer *et al.* (2008). Briefly, cultures were grown overnight in leucine-limited media (15 mg/l leucine) at 30°C and then subcultured the next day into fresh leucine-limited media. Samples were taken at the indicated time points. A series of 10-fold serial dilutions were prepared in a 96-well plate and then spot-plated onto YPD media.

Yeast strain construction

All strains were made in a *GAL*$^+$, *HAP1*-repaired, prototrophic derivative of S288C (Supplemental Table 5). The original strain was a kind gift from the Winston lab (Harvard Medical School), where it was constructed and designated FY2648 (Hickman and Winston, 2007; Hickman *et al.*, 2011). Gene deletions were constructed by transforming PCR products amplified from plasmids containing different deletion cassettes: pFA6a-kanMX for kanMX, pAG32 for hphMX, and pAC372 for natAC (Wach *et al.*, 1994; Lorenz *et al.*, 1995; Goldstein and McCusker, 1999). The plasmid pAC372 was a kind gift from Amy Caudy (University of Toronto), and the natAC cassette includes a yeast-codon–optimized nourseothricin-resistance gene, flanked by the same *Ashbya gossypii TEF* promoter and 3′ UTR in the other MX cassettes. Primers were designed with 40 flanking base pairs identical to the upstream and downstream region of genes to be deleted by homologous recombination. All gene deletions were made by transformation into a diploid to get a heterozygote, which was confirmed by PCR and then dissected to get MAT**a** and MAT α segregants. All combinatorial gene deletion/insertion strains were made by mating, sporulating, and tetrad dissection. Auxotrophic alleles of *LEU2* and *URA3* crossed into these strains were originally described by Brachmann *et al.* (1998). The pHluorin2 and mScarlet strains were constructed by transformation of a construct containing the *TDH3* promoter upstream of either pHluorin2 or mScarlet into the *CAN1* locus of haploid parents. Strains were confirmed by canavanine selection, PCR amplification of either pHluorin2 or mScarlet from the *CAN1* locus, fluorescence, and Sanger sequencing of the entire locus. All combinatorial gene deletion/insertion strains were made by mating, sporulation, and tetrad dissection. Sporulation was performed by growing cells to log phase in rich media, collecting cells by centrifugation, washing them once in 1% potassium acetate, and then resuspending them in 1% potassium acetate. Cells were then incubated at room temperature on a roller wheel for at least 4 d before tetrad dissection.

Genetic suppressor screen

All screens were performed by growing independent cultures of a MAT**a** and MATα version of each mutant overnight in YNB + glucose, followed by dilution into fresh YNB + glucose at a concentration of 10^2 cells/ml. This solution was dispensed into a 96-well plate (100 µl per well, roughly 10 cells per well), and because of the low dilution, each well was treated as an independent culture for the purposes of generating suppressor mutations. Each plate contained a single ETC mutant strain and an equal number of wells for each mating type. Plates were incubated with shaking at 30°C for 7 d. For each strain, 72 of the resulting cultures were plated in their entirety onto YPD to identify starvation suppressors. The remaining 24 cultures were pooled to measure cell density and estimate the number of cell divisions that had occurred for calculation of mutation rate (Lang, 2018). A single colony was patched from each culture with suppressors (unless there were too many colonies to identify an independent colony, as seen in "jackpot" mutation cultures).

Suppression was then confirmed by repeating the suppressor identification assay and comparing CFUs to ETC deletion strain parents. In the end, 131 independent suppressors were selected for whole genome sequencing, along with ETC mutant parent strains for comparison. Genomic DNA libraries were prepared using the TruSeq DNA library prep kit (Illumina) and sequenced using an Illumina HiSeq 2500 to an average coverage depth of 200×. Illumina adapters were trimmed from the reads by Trimmomatic, and the reads were aligned to the *S. cerevisiae* reference genome (R64.2.1; www.yeastgenome.org) using BWA-MEM with default options selected (Li, 2013; Bolger *et al.*, 2014). Potential variants unique to suppressor strains were identified using freebayes (Garrison and Marth, 2012). All potential variants were manually examined in an Integrative Genomics Viewer (Robinson *et al.*, 2012; Thorvaldsdóttir *et al.*, 2012). Potentially causative mutations were identified for ~90% of the suppressors.

RNA extraction, RNA-seq, and gene expression analysis

For RNA-seq, samples were collected for RNA extraction by vacuum filtration onto nylon filters. Filters were immediately placed into tubes, submerged into liquid nitrogen, and stored at –80°C until RNA extraction. RNA was extracted by the acid-phenol method. Briefly, samples were resuspended in 500 µl of lysis buffer (10 mM EDTA, 0.5% SDS, 10 mM Tris, pH = 7.5) and 500 µl of acidified phenol (pH = 4.3). Samples were then incubated at 65°C for 60 min with agitation every 5 min. For the ETC growth curve, samples for RNA extraction were collected at 0, 2, 4, 5, 6, 7, 8, 9, 10, 11, 12, 13, 14, 15, 16, 18, 20, 22, 24, 28, 32, 38, 46, and 58 h. Samples were cleaned using the Direct-Zol MiniPrep Plus kit according to manufacturer instructions (Zymo Research). For ETC suppressors, samples were collected for RNA extraction at one point before diauxic shift (t1, 4 h) and two points after diauxic shift (t2 and t3, 16 and 20 h, respectively). RNA was isolated identically, though the RNA was purified using Direct-zol-96 MagBeads according to manufacturer instructions (Zymo Research). RNA quality and concentration were assayed using a Fragment Analyzer instrument. RNA-seq libraries were prepared using the TruSeq Stranded Total RNA kit paired with the Ribo-Zero rRNA removal kit (Illumina). Libraries were sequenced on an Illumina HiSeq 4000 instrument. Basecalls were performed using CASAVA version 1.4 (Illumina). Reads were demultiplexed into fastq files using bcl2fastq2 v2.20.0.422. TPMs were calculated from fastq files using Salmon v0.91 and the "-noEffectiveLengthCorrection option" and the default transcriptome from the Saccharomyces Genome Database corresponding to genome build SacCer3 (The Bioconductor Dev Team, 2014). Differential expression analysis (related to Figure 6) was performed using Sleuth (Pimentel *et al.*, 2017). Briefly, the model used in Sleuth was "~cox4 + coq2 + cox4:ras2 + cox4:rts1 + cox4:tco89 + coq2:ras2 + coq2:rts1 + coq2:tco89" (":" indicates an interacting term, so cox4:ras2 will ask whether the cox4 ras2 double mutant is significantly different from the cox4 mutant; the cox4 mutant, on the other hand, is compared with wild type). This model was run twice, once on pre–diauxic shift samples and once on post–diauxic shift samples. The call to Sleuth, including specified parameters, was sleuth_prep(s2c, as.formula(model), min_reads = 2, min_prop = 0.2, target_mapping = t2g, read_bootstrap_tpm = TRUE, extra_bootstrap_summary = TRUE).

Transcriptional activity inference was performed using the Transfactivity program from the REDUCE suite on the TPM value matrix, floored at one TPM and row-normalized against the mean value (Bussemaker *et al.*, 2001). The position-specific affinity matrix (PSAM) list was obtained from YeTFaSCo expert-curated motifs (http://yetfasco.ccbr.utoronto.ca/1.02/Downloads/Expert_PFMs.zip) along with a promoter file containing up to a 600 base pair promoter sequence for each gene (for genes with fewer than 600 base pairs between the neighboring gene, the full intergenic, noncoding sequence was used) (de Boer and Hughes, 2012). For visualization, transcription factor activity coefficient values were rescaled between –1 and 1 for each motif by dividing each motif value by its own largest absolute value, allowing easier comparison between different transcription factor activities. For production of transcription factor activity heat maps, only motifs with an uncorrected $p < 0.0001$ in at least four samples were shown as significant (Supplemental Figures 2 and 6).

For the ETC growth curve, each time-series experiment was first floored at three TPM and then zero-normalized before hierarchical clustering was performed (Pearson uncentered metric, average linkage) using Cluster 3.0 (http://bonsai.hgc.jp/~mdehoon/software/cluster/) (de Hoon *et al.*, 2004). Nonnormalized time-zero data were also compared to confirm that no significant changes were present; most changes were relatively low fold change and appeared to be related to the slower growth rate observed in ETC mutants (Supplemental Figure 11). Data were visually represented, examined, and exported using Java TreeView version 1.1.6r2 (http://jtreeview.sourceforge.net/) (Saldanha, 2004).

Measurement of cytosolic pH

For pHluorin2-based measurements, strains with and without *TDH3* promoter–driven pHluorin2 integrated into the *CAN1* locus were grown overnight in YNB + glucose. Overnight cultures were then diluted to an $OD_{600} = 0.1$ in YNB + glucose. Cultures of each strain (200 µl) were run in a Costar 96-well plate in a BioTek model Synergy H1 Hybrid Reader plate reader (BioTek). The plate reader incubation was performed for 48 h with the following parameters: 30°C, double-orbital continuous shaking, and measurements every 15 min of OD_{600} (for cell density), ex. 470 nm/em. 510 nm, and ex. 395 nm/em. 510 nm (for pHluorin2). Background autofluorescence was removed using values from the non–pHluorin2 containing strains, and then the 470:395 ratio was used to estimate pH based on a standard curve. Three biological replicates were performed for each strain. To generate the standard curve, permeabilized cells were incubated in pH standards ranging from 5.5 to 8.0, with 0.5 pH unit intervals essentially as described (Carmody, 1961). Briefly, 40 µl aliquots of cells ($OD_{600} = 5$) were combined with 158 µl of pH buffer and 2 µl of 10% digitonin in dimethyl sulfoxide and then incubated for 10 min at room temperature (Carmody, 1961). Fluorescence measurements were performed as described above, including samples for background autofluorescence. Five technical replicates were averaged for two separate biological replicates for each pH standard for each strain analyzed. Using Microsoft Excel, a polynomial equation was fitted to the resulting standard curve for the pH range 5.5–8.0: $y = 1.241x^2 - 4.1309x + 8.9791$, where y is the calculated intracellular pH and x is the ratiometric pHluorin2 value (Supplemental Figure 7).

For mScarlet fluorescence lifetime imaging, time-resolved images were acquired on an SP8 confocal microscope (Leica Biosystems) and analyzed using PicoQuant software. For simplicity in the quantification, because mScarlet fluorescence displays a double exponential decay, we used the average photon arrival time as the readout instead of fitting the data. A total of 1500 photons at the maximum pixel value were collected per decay measurement. Samples were excited at 561 nm at 40 MHz using a HC PL APO CS 40×/0.85 objective at laser intensities that maintained a collection rate below 1000 kcounts/s on a HyD SMD detector. The emission window was 579–750 nm. For calibration, 500 photons were collected from permeabilized samples as described above for a pH

range from 4.0 to 8.0. For display of mean photon arrival times, we applied a Gaussian filter of 500 nm using PicoQuant software. The images were exported for analysis using FIJI (Schindelin *et al*., 2012). Segmentation of yeast was performed using the auto-threshold and watershed functions on the intensity images, and the regions of interest were used to calculate the mean of the average photon arrival time per yeast. Conversion of the mean photon arrival time to pH was performed by interpolation on the calibration curve values in Python.

Confirmation of mitochondrial genome stability in ETC mutants

Multiple studies have suggested that loss-of-function mutations in ETC components can lead to destabilization of mtDNA, potentially converting a single nuclear gene deletion strain into a rho^0 strain (Merz and Westermann, 2009; Zhang and Singh, 2014; Stenger *et al*., 2020). Among ETC complex genes, it is notable that these cases are often restricted to mutations associated with mitochondrial ATP synthase function (complex V), which suggests that this phenomenon may not be associated with all ETC gene deletions, but perhaps only those that result in destabilized membrane potential across the inner mitochondrial membrane (Contamine and Picard, 2000; Wang *et al*., 2007). Although the ETC mutants presented here did not exhibit the slow growth or colony size phenotypes associated with complete ablation of the mitochondrial genome, we used PCR to test whether two of our ETC mutants still contained mtDNA. Both *coq2*Δ and *cox4*Δ mutants still maintained mitochondrial genome integrity based on amplification of three different genes encoded in the mitochondrial genome (Supplemental Figure 12).

Data accessibility

All raw RNA-seq data for both the ETC growth curve and ETC suppressor gene expression experiments are available for download from gene expression omnibus (GEO) (GEO accession numbers GSE140353 and GSE140352, respectively). Additionally, a number of files are available to download associated with these articles. Details about each file and their contents can be found in the Supplemental "Downloadable Data Files Summary" document, also available for download. Briefly, these files include the TPM files associated with RNA-seq for both the ETC growth curve and ETC suppressor gene expression experiment, transcription factor activity coefficients and *p* values associated with REDUCE analysis for both RNA-seq data sets, and files associated with the differential gene expression analysis performed on the ETC suppressor RNA-seq data using SLEUTH (sample covariates file, SLEUTH results file, and a file containing lists of differentially expressed genes described in the article and shown in Figure 6).

ACKNOWLEDGMENTS

We thank members of the Calico yeast group and the Gibney lab for collaborative assistance and helpful discussion. We thank Andrea Ireland and Margaret Roy for Illumina library preparation and sequencing. We also thank Dan Gottschling and Andy York for manuscript comments and project support. This research was supported by Calico Life Sciences LLC and start-up funds provided to P.A.G. by Cornell University.

REFERENCES

Akdoğan E, Tardu M, Garipler G, Baytek G, Kavakli IH, Dunn CD (2016). Reduced glucose sensation can increase the fitness of Saccharomyces cerevisiae lacking mitochondrial DNA. PLoS One 11, 1–32.

Bindels DS, Haarbosch L, van Weeren L, Postma M, Wiese KE, Mastop M, Aumonier S, Gotthard G, Royant A, Hink MA, Gadella TWJ (2017). mScarlet: a bright monomeric red fluorescent protein for cellular imaging. Nat Methods 14, 53–56.

Boer VM, Amini S, Botstein D (2008). Influence of genotype and nutrition on survival and metabolism of starving yeast. Proc Natl Acad Soc USA 105, 6930–6935.

Bolger AM, Lohse M, Usadel B (2014). Trimmomatic: a flexible trimmer for Illumina sequence data. Bioinformatics 30, 2114–2120.

Boy-Marcotte E, Perrot M, Bussereau F, Boucherie H, Jacquet M (1998). Msn2p and Msn4p control a large number of genes induced at the diauxic transition which are repressed by cyclic AMP in Saccharomyces cerevisiae. J Bacteriol 180, 1044–1052.

Brachmann CB, Davies A, Cost GJ, Caputo E, Li J, Hieter P, Boeke JD (1998). Designer deletion strains derived from Saccharomyces cerevisiae S288C: a useful set of strains and plasmids for PCR-mediated gene disruption and other applications. Yeast 14, 115–132.

Brauer MJ, Huttenhower C, Airoldi EM, Rosenstein R, Matese JC, Gresham D, Boer VM, Troyanskaya OG, Botstein D (2008). Coordination of growth rate, cell cycle, stress response, and metabolic activity in yeast. Mol Biol Cell 19, 352–367.

Brauer MJ, Saldanha AJ, Dolinski K, Botstein D (2005). Homeostatic adjustment and metabolic remodeling in glucose-limited yeast culture. Mol Biol Cell 16, 2503–2517.

Broach JR (2012). Nutritional control of growth and development in yeast. Genetics 192, 73–105.

Bussemaker HJ, Li H, Siggia ED (2001). Regulatory element detection using correlation with expression. Nat Genet 27, 167–171.

Cai J, Yang J, Jones DP (1998). Mitochondrial control of apoptosis: the role of cytochrome c. Biochim Biophys Acta 1366, 139–149.

Calvo SE, Mootha VK (2010). The mitochondrial proteome and human disease. Annu Rev Genomics Hum Genet 11, 25–44.

Carmody WR (1961). An easily prepared wide range buffer series. J Chem Educ 38, 559–560.

Charoenbhakdi S, Dokpikul T, Burphan T, Techo T, Auesukaree C (2016). Vacuolar H+-ATPase protects Saccharomyces cerevisiae cells against ethano-linduced oxidative and cell wall stresses. Appl Environ Microbiol 82, 3121–3130.

Contamine V, Picard M (2000). Maintenance and integrity of the mitochondrial genome: a plethora of nuclear genes in the budding yeast. Microbiol Mol Biol Rev 64, 281–315.

Culbertson MR, Henry SA (1975). Inositol requiring mutants of Saccharomyces cerevisiae. Genetics 80, 23–40.

Da Cunha FM, Torelli NQ, Kowaltowski AJ (2015). Mitochondrial retrograde signaling: triggers, pathways, and outcomes. Oxid Med Cell Longev 2015, 482582.

de Boer CG, Hughes TR (2012). YeTFaSCo: a database of evaluated yeast transcription factor sequence specificities. Nucleic Acids Res 40, 169–179.

Dechant R, Binda M, Lee SS, Pelet S, Winderickx J, Peter M (2010). Cytosolic pH is a second messenger for glucose and regulates the PKA pathway through V-ATPase. EMBO J 29, 2515–2526.

de Hoon M, Imoto S, Nolan J, Miyano S (2004). Open source clustering software. Bioinformatics 20, 1453–1454.

Deprez MA, Eskes E, Wilms T, Ludovico P, Winderickx J (2018). pH homeostasis links the nutrient sensing PKA/TORC1/ScH9 ménage-à-trois to stress tolerance and longevity. Microb Cell 5, 119–136.

Di Bartolomeo F, Malina C, Campbell K, Mormino M, Fuchs J, Vorontsov E, Gustafsson CM, Nielsen J (2020). Absolute yeast mitochondrial proteome quantification reveals trade-off between biosynthesis and energy generation during diauxic shift. Proc Natl Acad Sci USA 117, 7524–7535.

Dolz-Edo L, van der Deen M, Brul S, Smits GJ (2019). Caloric restriction controls stationary phase survival through protein kinase A (PKA) and cytosolic pH. Aging Cell 18, e12921.

Estruch F (2000). Stress-controlled transcription factors, stress-induced genes and stress tolerance in budding yeast. FEMS Microbiol Rev 24, 469–486.

Galdieri L, Mehrotra S, Yu S, Vancura A (2010). Transcriptional regulation in yeast during diauxic shift and stationary phase. Omics 14, 629–638.

Garrison E, Marth G (2012). Haplotype-based variant detection from short-read sequencing. ArXiv, 1207.3907, 1–9.

Gasch AP, Spellman PT, Kao CM, Carmel-Harel O, Eisen MB, Storz G, Botstein D, Brown PO (2000). Genomic expression programs in the

response of yeast cells to environmental changes. Mol Biol Cell 11, 4241–4257.
Gibney PA, Hickman MJ, Bradley PH, Matese JC, Botstein D (2013). Phylogenetic portrait of the Saccharomyces cerevisiae functional genome. G3 (Bethesda) 3, 1335–1340.
Goldstein AL, McCusker JH (1999). Three new dominant drug resistance cassettes for gene disruption in Saccharomyces cerevisiae. Yeast 15, 1541–1553.
Görner W, Durchschlag E, Wolf J, Brown EL, Ammerer G, Ruis H, Schüller C (2002). Acute glucose starvation activates the nuclear localization signal of a stress-specific yeast transcription factor. EMBO J 21, 135–144.
Gresham D, Boer VM, Caudy A, Ziv N, Brandt NJ, Storey JD, Botstein D (2011). System-level analysis of genes and functions affecting survival during nutrient starvation in Saccharomyces cerevisiae. Genetics 187, 299–317.
Hacioglu E, Demir AB, Koc A (2012). Identification of respiratory chain gene mutations that shorten replicative life span in yeast. Exp Gerontol 47, 149–153.
Haurie V, Perrot M, Mini T, Jenö P, Sagliocco F, Boucherie H (2001). The transcriptional activator Cat8p provides a major contribution to the reprogramming of carbon metabolism during the diauxic shift in Saccharomyces cerevisiae. J Biol Chem 276, 76–85.
Henderson KA, Hughes AL, Gottschling DE (2014). Mother-daughter asymmetry of pH underlies aging and rejuvenation in yeast. eLife 3, 1–13.
Hickman MJ, Spatt D, Winston F (2011). The Hog1 mitogen-activated protein kinase mediates a hypoxic response in Saccharomyces cerevisiae. Genetics 188, 325–338.
Hickman MJ, Winston F (2007). Heme levels switch the function of Hap1 of Saccharomyces cerevisiae between transcriptional activator and transcriptional repressor. Mol Cell Biol 27, 7414–7424.
Isom DG, Page SC, Collins LB, Kapolka NJ, Taghon GJ, Dohlman HG (2018). Coordinated regulation of intracellular pH by two glucose-sensing pathways in yeast. J Biol Chem 293, 2318–2329.
Jazwinski SM (2013). The retrograde response: when mitochondrial quality control is not enough. Biochim Biophys Acta 1833, 400–409.
Joyner RP, Tang JH, Helenius J, Dultz E, Brune C, Holt LJ, Huet S, Müller DJ, Weis K (2016). A glucose-starvation response regulates the diffusion of macromolecules. eLife 5, 1–26.
Kawai S, Urban J, Piccolis M, Panchaud N, de Virgilio C, Loewith R (2011). Mitochondrial genomic dysfunction causes dephosphorylation of Sch9 in the yeast Saccharomyces cerevisiae. Eukaryot Cell 10, 1367–1369.
Kirchman PA, Kim S, Lai C, Jazwinski SM (1999). Interorganelle signaling is a determinant of longevity in Saccharomyces cerevisiae. Genetics 152, 179–190.
Kwon YY, Choi KM, Cho CY, Lee CK (2015). Mitochondrial efficiency-dependent viability of Saccharomyces cerevisiae mutants carrying individual electron transport chain component deletions. Mol Cells 38, 1054–1063.
Lang G (2018). Measuring mutation rates using the Luria-Delbrück fluctuation assay. Methods Mol Biol 1672, 21–32.
Leemputte FV, Vanthienen W, Wijnants S, Zeebroeck GV, Thevelein JM (2020). Aberrant intracellular pH regulation limiting glyceraldehyde-3-phosphate dehydrogenase activity in the glucose-sensitive yeast tps1Δ mutant. MBio 11, e02199-20.
Li H (2013). Aligning sequence reads, clone sequences and assembly contigs with BWA-MEM. ArXiv, 13033997, 1–3.
Liu Z, Butow RA (2006). Mitochondrial retrograde signaling. Annu Rev Genet 40, 159–185.
Liu Z, Sekito T, Epstein CB, Butow RA (2001). RTG-dependent mitochondria to nucleus signaling is negatively regulated by the seven WD-repeat protein Lst8p. EMBO J 20, 7209–7219.
Longo VD, Shadel GS, Kaeberlein M, Kennedy B (2013). Replicative and chronological aging in Saccharomyces cerevisiae. Cell Metab 16, 18–31.
López-Otín C, Blasco MA, Partridge L, Serrano M, Kroemer G (2013). The hallmarks of aging. Cell 153, 1194–1217.
Lorenz MC, Muir RS, Lim E, McElver J, Weber SC, Heitman J (1995). Gene disruption with PCR products in Saccharomyces cerevisiae. Gene 158, 113–117.
Mahon MJ (2011). pHluorin2: an enhanced, ratiometric, pH-sensitive green florescent protein. Adv Biosci Biotechnol 2, 132–137.
Malina C, Larsson C, Nielsen J (2018). Yeast mitochondria: an overview of mitochondrial biology and the potential of mitochondrial systems biology. FEMS Yeast Res 18, 1–17.
Martin J, Mahlke K, Pfanner N (1991). Role of an energized inner membrane in mitochondrial protein import. J Biol Chem 266, 18051–18057.
Martínez-Muñoz GA, Kane P (2008). Vacuolar and plasma membrane proton pumps collaborate to achieve cytosolic pH homeostasis in yeast. J Biol Chem 283, 20309–20319.
Martinez-Pastor M, Marchler G, Schuller C, Marchler-Bauer A, Ruis H, Estruch F (1996). The Saccharomyces cerevisiae zinc finger proteins Msn2p and Msn4p are required for transcriptional induction through the stress-response element (STRE). EMBO J 15, 2227–2235.
Matsuura A, Anraku Y (1993). Characterization of the MKS1 gene, a new negative regulator of the Ras-cyclic AMP pathway in Saccharomyces cerevislae. Mol Gen Genet 238, 6–16.
McCormick MA, Delaney JR, Tsuchiya M, Tsuchiyama S, Shemorry A, Sim S, Chou AC, Ahmed U, Carr D, Murakiami CJ, *et al.* (2015). A comprehensive analysis of replicative lifespan in 4,698 single-gene deletion strains uncovers conserved mechanisms of aging. Cell Metab 22, 895–906.
Merz S, Westermann B (2009). Genome-wide deletion mutant analysis reveals genes required for respiratory growth, mitochondrial genome maintenance and mitochondrial protein synthesis in Saccharomyces cerevisiae. Genome Biol 10, R95.
Munder MC, Midtvedt D, Franzmann T, Nuske E, Otto O, Herbig M, Ulbricht E, Muller P, Taubenberger A, Maharana S, *et al.* (2016). A pH-driven transition of the cytoplasm from a fluid- to a solid-like state promotes entry into dormancy. eLife 5, 1–30.
Nunnari J, Suomalainen A (2012). Mitochondria: in sickness and in health. Cell 148, 1145–1159.
Ohkuni K, Hayashi M, Yamashita I (1998). Bicarbonate-mediated social communication stimulates meiosis and sporulation of Saccharomyces cerevisiae. Yeast 14, 623–631.
Orij R, Brul S, Smits GJ (2011). Intracellular pH is a tightly controlled signal in yeast. Biochim Biophys Acta 1810, 933–944.
Orij R, Postmus J, Beek AT, Brul S, Smits GJ (2009). In vivo measurement of cytosolic and mitochondrial pH using a pH-sensitive GFP derivative in Saccharomyces cerevisiae reveals a relation between intracellular pH and growth. Microbiology 155, 268–278.
Orij R, Urbanus ML, Vizeacoumar FJ, Giaever G, Boone C, Nislow C, Brul S, Smits GJ (2012). Genome-wide analysis of intracellular pH reveals quantitative control of cell division rate by pHc in Saccharomyces cerevisiae. Genome Biol 13, 1–15.
Ott M, Robertson JD, Gogvadze V, Zhivotovsky B, Orrenius S (2001). Cytochrome c release from mitochondria proceeds by a two-step process. Proc Natl Acad Sci USA 99, 1259–1263.
Petti AA, Crutch CA, Rabinowitz JD, Botstein D (2011). Survival of starving yeast is correlated with oxidative stress response and nonrespiratory mitochondrial function. Proc Natl Acad Sci USA 108, E1089–E1098.
Petti AA, McIsaac RS, Ho-Shing O, Bussemaker HJ, Botstein D (2012). Combinatorial control of diverse metabolic and physiological functions by transcriptional regulators of the yeast sulfur assimilation pathway. Mol Biol Cell 23, 3008–3024.
Pimentel H, Bray NL, Puente S, Melsted P, Pachter L (2017). Differential analysis of RNA-seq incorporating quantification uncertainty. Nat Methods 14, 687–690.
Powers RW III, Kaeberlein M, Caldwell SD, Kennedy BK, Fields S (2006). Extension of chronological life span in yeast by decreased TOR pathway signaling. Genes Dev 20, 174–184.
Rehling P, Model K, Brandner K, Kovermann P, Sickmann A, Meyer HE, Kühlbrandt W, Wagner R, Truscott KN, Pfanner N (2003). Protein insertion into the mitochondrial inner membrane by a twin-pore translocase. Science 299, 1747–1751.
Reiter W, Klopf E, Wever VD, Anrather D, Petryshyn A, Roetzer A, Niederacher G, Roitinger E, Donhal I, Gorner W, *et al.* (2013). Yeast protein phosphatase 2A-Cdc55 regulates the transcriptional response to hyperosmolarity stress by regulating Msn2 and Msn4 chromatin recruitment. Mol Cell Biol 33, 1057–1072.
Robinson JT, Thorvaldsdóttir H, Winckler W, Guttman M, Lander ES, Getz G, Mesirov JP (2012). Integrative genomics viewer. Nat Biotechnol 29, 24–26.
Saldanha AJ (2004). Java Treeview—extensible visualization of microarray data. Bioinformatics 20, 3246–3248.
Saldanha AJ, Brauer MJ, Botstein D (2004). Nutritional homeostasis in batch and steady-state culture of yeast. Mol Biol Cell 15, 4089–4104.
Saliba E, Evangelinos M, Gournas C, Corrillon F, Georis I, André B (2018). The yeast H+-ATPase pma1 promotes rag/gtr-dependent TORC1 activation in response to h+-coupled nutrient uptake. eLife 7, 1–27.
Santhanam A, Hartley A, Düvel K, Broach JR, Garrett S (2004). PP2A phosphatase activity is required for stress and Tor kinase regulation of yeast stress response factor Msn2p. Eukaryot Cell 3, 1261–1271.

Schindelin J, Arganda-Carreras I, Frise E, Kaynig V, Longair M, Pietzsch T, Preibisch S, Rueden C, Saalfeld S, Schmid B, *et al*. (2012). Fiji: an open-source platform for biological-image analysis. Nat Methods 9, 676–682.
Shakoury-Elizeh M, Tiedeman J, Rashford J, Ferea T, Demeter J, Garcia E, Rolfes R, Brown PO, Botstein D, Philpott CC (2004). Transcriptional remodeling in response to iron deprivation in Saccharomyces cerevisiae. Mol Biol Cell 15, 1233–1243.
Smith CP, Thorsness PE (2005). Formation of an energized inner membrane in mitochondria with a γ-deficient F1-ATPase. Eukaryot Cell 4, 2078–2086.
Stenger M, Le DT, Klecker T, Westermann B (2020). Systematic analysis of nuclear gene function in respiratory growth and expression of the mitochondrial genome in S. cerevisiae. Microb Cell 7, 234–249.
The Bioconductor Dev Team (2014). BSgenome.Scerevisiae.UCSC.sacCer3: Saccharomyces cerevisiae (Yeast) Full genome (UCSC version sacCer3), R package version 1.4.0.
Thorvaldsdóttir H, James T, Jill P (2012). Integrative Genomics Viewer (IGV): high-performance genomics data visualization and exploration. Brief Bioinform 14, 178–192.
Vafai SB, Mootha VK (2012). Mitochondrial disorders as windows into an ancient organelle. Nature 491, 374–383.
Wach A, Brachat A, Pöhlmann R, Philippsen P (1994). New heterologous modules for classical or PCR-based gene disruptions in Saccharomyces cerevisiae. Yeast 10, 1793–1808.
Wang Y, Singh U, Mueller DM (2007). Mitochondrial genome integrity mutations uncouple the yeast Saccharomyces cerevisiae ATP synthase. J Biol Chem 282, 8228–8236.
Werner-Washburne M, Braun E, Johnston GC, Singer RA (1993). Stationary phase in the yeast Saccharomyces cerevisiae. Microbiol Rev 57, 383–401.
Yamaguchi-Iwai Y, Dancis A, Klausner RD (1995). AFT: a mediator of iron regulated transcriptional control in Saccharomyces cerevisiae. EMBO J 14, 1231–1239.
Zampar GG, Kümmel A, Ewald J, Jol S, Niebel B, Picotti P, Aebersold R, Sauer U, Zamboni N, Heinemann M (2013). Temporal system-level organization of the switch from glycolytic to gluconeogenic operation in yeast. Mol Syst Biol 9, 651.
Zhang H, Singh KK (2014). Global genetic determinants of mitochondrial DNA copy number. PLoS One 9, 1–12.